IEEE Access
Multidisciplinary | Rapid Review | Open Access Journal

Received July 21, 2020, accepted August 3, 2020, date of publication August 17, 2020, date of current version August 28, 2020.

Digital Object Identifier 10.1109/ACCESS.2020.3017217

Deterioration Behavior Analysis and LSTM-Based Failure Prediction of GIB Electrical Contact Inside Various Insulation Gases

XIANGYU GUAN[1], YUEQUAN WEN[1], ZHE DONG[1], NAIQIU SHU[2], HUI PENG[2], WEI GAO[3], (Member, IEEE), AND DAVID WENZHONG GAO[3], (Senior Member, IEEE)

[1]School of Electrical Engineering and Automation, Fuzhou University, Fuzhou 350108, China
[2]School of Electrical Engineering and Automation, Wuhan University, Wuhan 430072, China
[3]Department of Electrical and Computer Engineering, University of Denver, Denver, CO 80208, USA

Corresponding author: Xiangyu Guan (xiangyuguan1986@163.com)

This work was supported in part by the National Science Foundation of China under Grant 51607124, and in part by the China Scholarship Council under Grant 201806275047.

ABSTRACT Plug-in connector of gas insulated bus (GIB) could be subject to the wear and electrical contact resistance (ECR) deterioration processes under cyclic mechanical and current loads. A specific test platform is designed to simulate the current-carrying wear and ECR degradation process of Ag-plated GIB electrical contact spot inside SF6, N2 and Air insulation mediums under current loads. Worn surface morphology and chemical composition are observed and analyzed. Influence of insulation medium and current load on deterioration mechanism of GIB electrical contact are discussed. Raw ECR curve obtained from current-carrying experiment is smoothed by the exponentially weighted moving average (EWMA) method. A long short-term memory (LSTM) neural network is then proposed to realize both single-step and multi-step ECR and failure predictions of GIB electrical contact. Results show that adhesive wear on contact surface happened due to materials transfer. Deterioration of contact spot inside air medium is much severer than those in SF6 and N2 due to oxidation effect. Deterioration of contact spot inside SF6 medium under high current load is severer than those under low current load due to the change of wear behavior and chemical reactions. Compared with other methods, LSTM could achieve better performance in both single-step and multi-step failure prediction of GIB electrical contact.

INDEX TERMS Electrical contact resistance (ECR), gas insulated bus (GIB), insulation gases, LSTM.

I. INTRODUCTION

The gas insulated bus (GIB) is an essential component of the gas insulated switchgear (GIS) and gas insulated line (GIL) as high-voltage and large-current power transmission apparatus. Slidable plug-in connector is used to realize electrical contact in bus connection of GIB equipment. Operation reliability of GIB equipment is dependent on contact status of plug-in connector [1]. Even overheating on several seriously deteriorated contact elements could induce melting, partial discharge and flashover of GIB equipment, then cause catastrophic consequences such as GIB equipment damage and power grid knock down [2], [3]. Influenced by the pressure-vessel insulation design, and cyclic mechanical and current loads during GIB equipment operation, contact interface of the GIB plug-in connector is subject to complex current-carrying wear processes [4]–[6]. In order to ensure the safety operation of GIB equipment, it is essential to study the deterioration behavior and ECR degradation process of GIB electrical contact inside various insulation gases under current loads thus in order to evaluate its health condition and residual useful life (RUL).

Current-carrying wear process could happen on closed electrical connector when two contact elements are subject to relative movements induced by cyclic mechanical and current loads [7], [8]. Wear behaviors and influence factors of various current-carrying contact pairs inside air atmosphere were researched in [9], [10]. Results show that the current-carrying wear behavior is influenced by contact materials, mechanical displacement, contact force and current loads. The ECR increase and contact deterioration process are related to the formation and accumulation of high resistivity oxidized wear

The associate editor coordinating the review of this manuscript and approving it for publication was Xiao-Sheng Si.

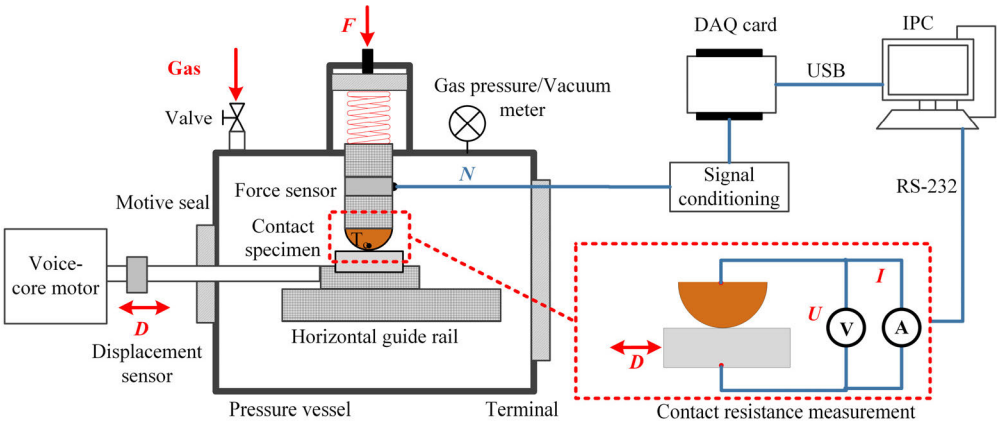

FIGURE 1. Schematic diagram of current-carrying wear experiment platform and contact resistance measurement.

debris inside contact zone. Atmosphere is one critical factor that could influence current-carrying wear behaviors. Atmosphere and gas pressure could influence friction behavior of pure metals through chemisorption on metal contact surface [11]. Influence of test atmospheres on tribological behavior of different electrical contacts with surface coatings was studied in [12]–[14]. Results show that atmosphere could react with contact metals, and the chemical surface film could influence the wear processes and ECR degradation behaviors. However, due to usage of special SF6 gas and large operation currents, current-carrying wear behavior of GIB contact has attracted few previous attentions.

Failure prediction is an essential aspect for the reliability design, and maintenance of electrical contact. Several failure prediction methods were applied on various type of electrical contacts. A failure prediction method of circular electrical connector by oxide-film accumulation mechanism and particle filter method was introduced in [15]. Residual life of electrical connector predicted by intermitted failure and hidden Semi-Markov model was introduced in [16]. Electrical contact endurance of silver coating was defined by a modified Archard law in [17]. Machine learning technology has also attracted attention on the electrical endurance and failure prediction of electrical connectors [18]. Reliability of electrical contact could strongly affect the safe operation of GIB equipment. However, current service life evaluation of GIB contact only considered wear of sliver coating under the constant daily cyclic mechanical loads [19], and there is still no effective failure prediction method of GIB electrical contact due to the lack of deterioration behavior research and ECR degradation dataset.

The main aim of this work is to reveal the contact deterioration behavior and develop a failure prediction method of GIB electrical contact inside different insulation gases under mechanical and current loads. This is a specific application involving current-carrying wear and electrical contact. However, the wear behavior and ECR deterioration process of electrical contact play essential roles in reliability design, installation and operation maintenance of GIB equipment. Thus, research on the wear deterioration behavior and failure prediction method of GIB electrical contact have both theorical and application significances.

This paper is organized as follows: In section 2, a specific current-carrying wear experiment platform is designed first to measure ECR degradation curve of GIB contact specimen inside different insulation gases subject to cyclic mechanical and current loads. In section 3, failure mechanisms of contact specimen are discussed by the surface morphology inspection and chemical composition analysis. In section 4, contact failure threshold, raw ECR data smoothing, and failure prediction algorithm are introduced. Architecture of LSTM model is given in section 5. Model merits comparison, both single-step and multi-step ECR and failure prediction results are discussed in section 6.

II. EXPERIMENT SET-UP

A specific current-carrying wear physical experiment platform (Fig.1) was designed to investigate the contact degradation process and deterioration behaviors of GIB contact inside different insulation gases, mimicking the operation environment of GIB equipment. Contact specimen with comparable structure of prototype GIB electrical contact consists of the upper copper contact element and the lower aluminum contact element. Contact surface is plated with silver to enhance electrical conductivity. The lower contact element (movable contact) is fixated on a horizonal guide rail. Controlled constant amplitude sinusoidal wave mechanical cyclic displacement load is applied by a voice-core motor with displacement sensor (grating ruler). The voice-core motor is attached to horizonal guide rail via a shaft through the motive seal on left side of the pressure vessel. The upper contact element is attached to spring force adjuster to provide normal contact force. A force sensor is adopted to measure normal contact force. Different insulation gases sealed inside the pressure vessel are inflated through gas valve.

A. CONTACT SPECIMEN CONFIGURATION

Typical GIB capsule includes metal tank, insulator, bus conductor and plug-in connector (Fig.2(a)). Electrical insulation of GIB capsule is realized by insulation gas and insulator. Plug-in connector consists of tens of parallel contact elements to separate large load current (more than 1kA), and operation current on each contact element is normal tens of amperes. Due to electrical contact resistance and temperature rise, contact spot has the worst working condition. To avoid the system complexity and uncertain results of entire GIB connector, single contact spot of GIB connector was selected as contact specimen (Fig.2(b)). Copper static contact element is represented by the upper contact specimen. Aluminum movable contact element is represented by the lower contact specimen. Parameters of contact specimen are listed in Table. 1.

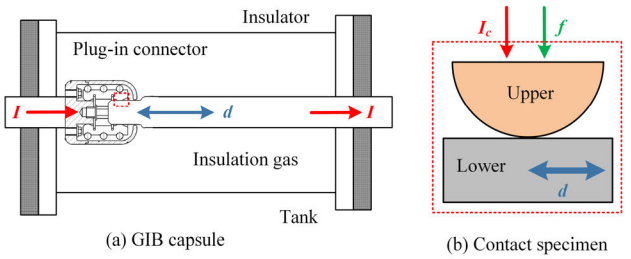

FIGURE 2. Schematic structure of GIB and electrical contact specimen.

TABLE 1. Parameters of GIB contact specimen.

Upper contact material	Aluminum alloy 6063-T6
Lower contact material	Copper T2Y
Plated material	Sliver
Plated thickness(μm)	20
Upper contact radius (mm)	10
Upper contact thickness (mm)	4
Lower contact radius (mm)	50
Lower contact length (mm)	20
Lower contact height (mm)	10

B. CONTACT RESISTANCE MEASUREMENT

A 4-point method is used to measure the ECR of GIB electrical contact specimen based on Ohm's law (Fig.1). Constant test current is supplied by a programmable current source (range 250A, precision 0.1A). Contact voltage drop between contact specimen was measured by a 6 1/2 digital microvolt meter (Keithley 2000, voltage resolution 0.1μV). Contact resistance are then calculated by the division of contact voltage drop with respect to test current.

Connection wires of force sensor, current source and voltage meter are expanded out the sealed electrical terminals on the right side of the pressure vessel. Programable current source and digital microvolt meter are connected to an industrial personal computer (IPC) through RS-232 cables to record test current, voltage drop, and then calculate the ECR. Output of the force sensor is linked with data acquisition (DAQ) card through signal conditioning circuit. The DAQ card (Advantech-USB-4716, 16 channels, 16Bit, 200 kS/s) is connected to IPC through USB cables to record the contact force. The contact force and ECR are recorded by a dedicated software programmed by the LabVIEW platform.

C. EXPERIMENT PROCESS

Current-carrying experiment process of GIB electrical contact is as follows. First, upper and lower contact specimen are prepared and attached to the corresponding fixtures. To remove greases, dusts and oxidation layers on surface, contact specimen are cleaned by alcohol with ultra-sonic cleaner in advance. Second, pressure vessel is pumped to vacuum condition (residual gas pressure is 133Pa according to field installation requirement of GIB equipment [21]). 0.4 Mpa insulation gases are then inflated into pressure vessel, 12 hours waiting period is used to confirm no obvious gas leakage. Third, after ensuring all wires are correctly connected, and data acquisition system is initiated to record data. Experiment parameters (contact force, mechanical and current loads) are set and experiment begins. After the experiment, the contact specimen is sealed inside vacuum package for conducting worn surface morphology and chemical composite analysis.

III. CONTACT DETERIORATION ANALYSIS

Degradation behaviors of GIB electrical contact specimen inside different insulation gases under mechanical and current loads were simulated on designed current-carrying wear experiment platform. The current wear test conditions are as follows: cyclic relative displacement is sinewave with amplitude 500μm and 1 Hz frequency under low current load of 20A and high current load of 60A from typical daily mechanical and current loads of GIB capsule. Normal contact force amplitude is set as 30N according to design parameters of GIB plug-in connector [25]. Insulation gas is air, SF6 and N2. Gas pressure is set as 0.4Mpa according to insulation design of GIB equipment (SF_6), and gas pressure of air and N2 are also set as 0.4Mpa to maintain the pressure parameter. ECR sample interval is set as 10s during experiment to obtain enough sequence dataset. Worn surface morphology and material composition of contact specimen were observed and analyzed by the 3-D surface profiler, scanning electron microscope (SEM) and energy-dispersive X-ray spectroscopy (EDX) after experiment.

3-D Surface profile of GIB electrical contact specimen obtained by surface profiler after experiment with SF6 gas under 20A test current is shown in Fig.3. Results show that severe adhesion friction happened on the contact surface due to the differences of contact material harnesses. Worn surface is formed on the softer lower contact specimen (Aluminum alloy 6063T6 with the Young's module of 69 GPa). Wear debris which consist of softer sliver plate and aluminum are attached on the harder upper contact specimen (Copper T2Y with the Youngs's module of 110 GPa). Adhesion wear on

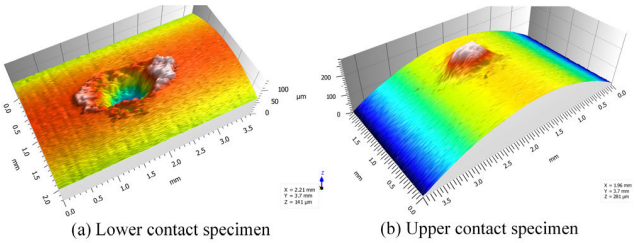

FIGURE 3. 3-D surface profile of GIB electrical contact specimen.

contact surface could break the silver coating and generate high-resistivity surface layer causing the ECR to increase.

A. INFLUENCE OF INSULATION GAS MEDIUM

For the complexity of current-carrying wear mechanisms influenced by mechanical wear/crack, chemical reaction and current-induced heating, ECR deterioration curves show nonlinear behaviors and only measured ECR values inside different insulation gases are focused and discussed. Raw ECR deterioration curves of GIB electrical contact inside different insulation gases under 60A current load are shown in Fig.4. Results show that the insulation gases affect the ECR deterioration curve: 1) ECR deterioration of contact specimen inside air is much severer than those in SF6 and N2 gases. This is mainly due to the strong oxidation effect and formation of high resistivity oxidation film on contact surface inside air. 2) ECR deterioration of contact specimen inside SF6 gas is severer than that inside N2 gas. This is probably due to the following reasons: the local heating on contact spot, SF6 gas decomposition [20]–[22], chemical reaction between SF6 decomposition product and contact material, and high resistivity chemical reaction product formed on contact surface.

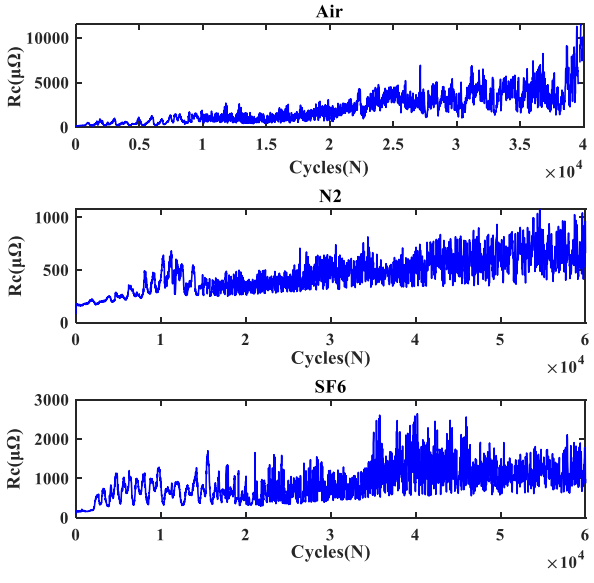

FIGURE 4. Raw ECR curves inside different insulation gases.

B. INFLUENCE OF LOAD CURRENT

Contact surface morphology and chemical composition of GIB contact specimen under 20A and 60A test currents inside SF_6 insulation gas are shown in Fig.5. Results show that under low test current (20A), mechanical wear is dominant on contact surface with obvious wear scar (SEM image of Fig.5(a)). Only contact metal and slight oxygen are found in EDX spectrum (Fig.5(a)), which indicates that no obvious chemical reaction happened between insulation gas and contact material. However, under the local heating by high test current (60A), the smooth scar morphology indicates that fusion welding has happened inside contact surface (SEM image of Fig.5(b)). Fluoride and sulphide composites besides contact metal are found in EDX spectrum (Fig.5(b)), which indicates that under local heating on contact surface by high load current, chemical reaction happens between SF6 decomposition product and contact materials [20]–[22], and high resistivity reaction product could accelerate contact deterioration process.

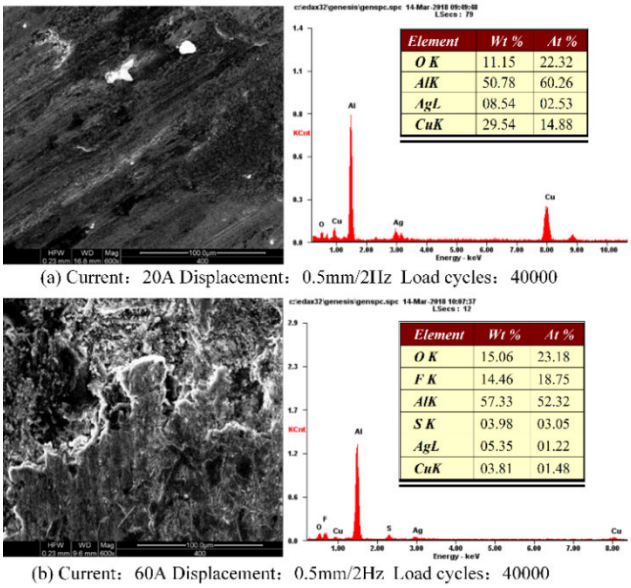

FIGURE 5. Surface morphology and chemical composition of GIB contact.

IV. FAILURE PREDICTION ALGORITHM

In order to evaluate operation reliability of GIB electrical contact, a failure prediction model based on LSTM neural network was developed. Overall framework of LSTM based RUL prediction process consisting of data processing, model construction and failure prediction is illustrated in Fig.6. During data processing stage, raw ECR curve is first obtained through the current-carrying wear experiment. Raw ECR curve is then smoothed and normalized. Processed ECR data is labeled and split into training dataset, validation dataset and test dataset. During model construction stage, the LSTM model is first trained on training dataset. By reducing the loss function between predicted result y and labeled result y' on

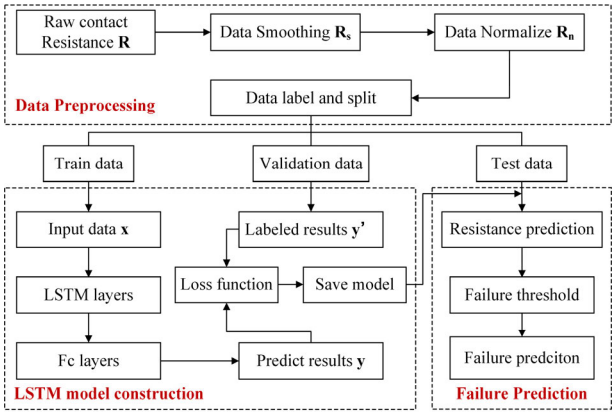

FIGURE 6. LSTM-based failure prediction process of GIB electrical contact.

validation dataset, parameters of LSTM model are updated and finally saved. During failure prediction stage, ECR is predicted using test dataset by the trained LSTM model and model merits was evaluated. The failure threshold of GIB electrical contact was defined and contact failure was then predicted by the cycle point when contact failure threshold reached.

A. CONTACT FAILURE THRESHOLD

The contact resistance could generate concentrated contact temperature rise on contact interface which is higher than other parts of GIB connector then decide its performance. Thermal performance is the main factor during design and maintenance of the high current carrying power connector. According to standard IEC 62271-1, the maximum allowed long-term operation temperature of Ag-plated electric power connector is 105°C [23].

The contact temperature rise is influenced by the contact voltage drop. Relationship between the contact temperature and contact resistance can be calculated by voltage-temperature (V-T) relation [24].

$$R_k = U_k/I = \sqrt{8L(T - T_b)\frac{(T + T_b)}{2}}/I \tag{1}$$

where U_k is contact voltage drop; I is operation current; L is Lorenz number which is 2.4×10.8 (V^2/K^2) [21]; T_c and T_b are the temperatures of contact and connector respectively.

In this work, we define long-term connector temperature T_b to be 398K (105°C) [23], contact temperature T_c to be 423K (soften temperature of aluminum alloy). Long term operation current I is 100A (minimum section area of each copper contact finger is 20mm^2 with 5A/mm^2). According the GIB contact design margin, the failure threshold of ECR value is set as 823.5$\mu\Omega$ which is 1.4 times of the results from the V-T relation [25].

B. ECR CURVE SMOOTHING

The raw ECR curve of GIB electrical contact includes both short-term and long-term trends. The short-term trend

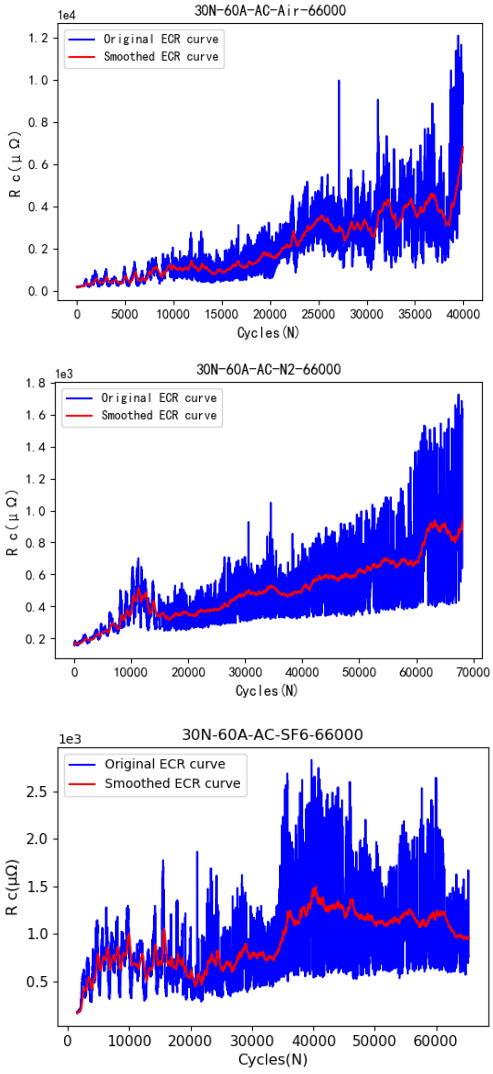

FIGURE 7. Smoothing of ECR curve.

mainly influenced by the ECR measurement fluctuation. The long-term trend indicates the ECR degradation process during equipment operation. During failure prediction analysis, we mainly concern the long-term degradation trend of GIB electrical contact. Thus, Raw ECR curve obtained from experiments should be smoothed to remove short-term trend before fed into the LSTM neural network. An exponentially weighted moving average (EWMA) is used in this work to obtain smoothed ECR curve and extract the long-term trend of raw ECR curve (Fig.7). Mathematical description of EWMA is shown as follows

$$R_t = \frac{\sum_{i=0}^{t} \omega_i r_{t-i}}{\sum_{i=0}^{t} \omega_i} \tag{2}$$

where r_t is the raw ECR sequence; R_t is the smoothed ECR sequence. Exponential weight ω_i is given as follows.

$$\omega_i = (1 - \alpha)^i, \quad \alpha = 2/(1 + s). \tag{3}$$

where s is the sequence span, in this paper $s = 50$.

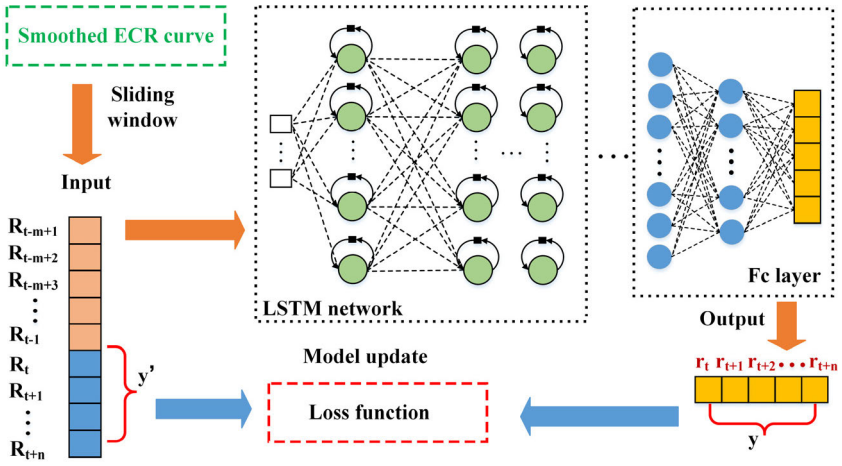

FIGURE 8. Architecture of LSTM-based failure prediction model.

V. ARCHITECTURE OF LSTM NEURAL NETWORK

ECR degradation curve of GIB electrical contact belongs to nonlinear time sequence. A LSTM neural network is introduced in this paper to realize ECR and RUL prediction of GIB electrical contact. Architecture of LSTM neural network is shown in Fig.8. Input sequence data was first generated from the smoothed ECR curve by sliding windows. One sliding window consists of m ECR values prior to time instant t (length of observation window), and n ECR values after time instant t (length of prediction window). The ECR sequence of observation window was first fed into multi LSTM layers to extract high dimension sequence features. A Fc neural network using high dimension sequence features as input was designed to output prediction ECR results. Model parameters were updated by reducing loss function between real ECR values and output predicted ECR values.

A. LSTM CELL

Long short-term memory (LSTM) is a modified recurrent neural network (RNN) using gate units to overcome gradient vanishing or gradient exploding problems [26]. Structure of LSTM cell is shown in Fig.9. A LSTM cell contains three gates: input gate, output gate and forget gate. Input gate $\mathbf{G_i}$ determines whether a new input x_t could be added to memory cell. Output gate $\mathbf{G_o}$ determines whether cell generates output u_t. Forget gate $\mathbf{G_f}$ determines whether the previous value c_{t-1} in memory cell is kept. Control signals of i_t (input gate), f_t (forget gate) and o_t (output gate) are given as follows.

$$\begin{cases} i_t = f_g\left(w_{xi}x_t + w_{ui}u_{t-1} + w_{ci}c_{t-1} + b_i\right) \\ f_t = f_g\left(w_{xf}x_t + w_{uf}u_{t-1} + w_{cf}c_{t-1} + b_f\right) \\ o_t = f_g\left(w_{xo}x_t + w_{uo}u_{t-1} + w_{co}c_t + b_o\right) \end{cases} \tag{4}$$

where x_t is input, u_{t-1} is previous output; c_{t-1} is previous value of memory cell; w_{xi}, w_{ui}, w_{ci} are weights of input gate; b_i is bias of input gate; w_{xf}, w_{uf}, w_{cf} are weights of forget gate; b_f is bias of forget gate; w_{xo}, w_{uo}, w_{co} are weights of output gate; bo is bias of output gate; f_g is activation function of gate unit. Updated LSTM memory cell value c_t and output u_t are given as follows

$$c_t = f_t \times c_{t-1} + i_t \times f_i\left(w_{xc}x_t + w_{uc}u_{t-1} + b_c\right) \tag{5}$$

$$u_t = o_t \times f_o\left(c_t\right) \tag{6}$$

where w_{xc}, w_{uc} are weights of input unit; b_c is bias of input unit; f_i and f_o are activation functions of input unit and output unit, respectively.

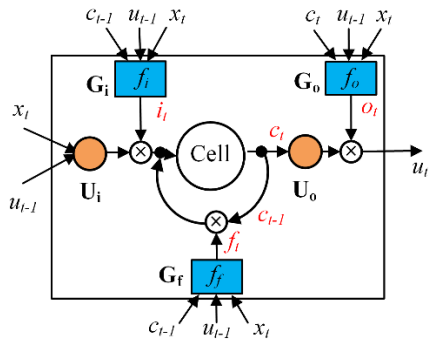

FIGURE 9. Architecture of LSTM cell.

B. FULLY CONNECTED NEURAL NETWORK

A fully connected (Fc) neural network is used in this work to output ECR prediction results. Mathematical description of fully connected neural layers is as follows

$$\mathrm{y} = f_n(wx + b) \tag{7}$$

where x is the output of forward LSTM network also as input of Fc neural network; w and b are weight and bias of neural cell. $f_n(.)$ is activation function of Fc layers.

C. ACTIVATION FUNCTION AND LOSS FUNCTION

Different activation functions are used in different layers of LSTM architecture. *ReLU* activation function is used in Fc

layers for its faster computational ability. *Sigmoid* activation function is used in LSTM gates to generate a control signal between (0,1). *Tanh* activation function is used in LSTM input/output units to decrease gradient vanishing or exploding problem. Mathematical descriptions of different activation functions are given as follows

$$\begin{cases} sigmoid(x) = 1/\left(1+e^{-x}\right) \\ Tanh(x) = \left(e^{x}-e^{-x}\right)/\left(e^{x}+e^{-x}\right) \\ ReLu(x) = \max(x,0) \end{cases} \tag{8}$$

During model evaluation process, hyperparameters of the LSTM model such as weights and biases are optimized by reducing loss function between real ECR values and output prediction values through gradient descent method.

VI. RESULTS AND DISCUSSION

LSTM-based failure prediction model of GIB electrical contact is built in this paper. Detailed model configuration is shown in Table 2. Total ECR curve was split to training dataset, validation dataset and test dataset. The training dataset and validation dataset was used to train the model. The independent test dataset was used to realize ECR prediction by the trained model. Sequence features of input ECR curve were extracted by multi LSTM layers. Extracted sequence features were then fed into fully connected (Fc) layers to output prediction results. 50% dropout were used to fight against overfitting problem. Loss function was minimized by the Adam optimizer. RUL prediction model was trained on a laptop workstation (Intel i7-8750, 32G RAM, NVidia p2000 GPU accelerator) under the Keras environment (Googles' TensorFlow backend). Length of observation window is 20, and length of prediction window is 5. Three other time sequence prediction methods including the autoregressive integrated moving average (ARIMA), the multilayer perceptron (MLP), and the convolutional neural network (CNN) were chosen to compare with performance of introduced method.

TABLE 2. Configuration of proposed LSTM model.

Input shape (20,1)				
Layer	Hidden Cells	Time Steps	Return	Output shape
LSTM1	128	20	-	(20,128)
LSTM2	64	-	-	(20,64)
Fc1	32	-	-	32
Fc2	-	-	-	5
Total Parameters: 301633				

Metrics of LSTM model was evaluated by THE root mean square percentage error (*RMSPE*), mean absolute percentage error (*MAPE*), and R-squared (*R_sq*) value which are defined as follows.

$$RMSPE = \sqrt{\frac{1}{N}\sum_{i=1}^{N}\left(\frac{\hat{y}_i - y_i}{\hat{y}_i}\right)^2} \tag{9}$$

$$MAPE = \frac{1}{N}\sum_{i=1}^{N}\left|\frac{\hat{y}_i - y_i}{\hat{y}_i}\right| \tag{10}$$

$$R\_sq = 1 - \frac{\sum_{i=1}^{N}(\hat{y}_i - y_i)^2}{\sum_{i=1}^{N}(\hat{y}_i - \bar{y})^2} \tag{11}$$

where $\hat{y}_i$ is the true ECR value; y_i is the LSTM model predicted ECR value; $\bar{y}$ is the mean value of true ECR.

A. SINGLE-STEP ECR PREDICTION

Single-step ECR prediction results of GIB electrical contact inside different insulation gases are shown in Fig.10. Performance of model metrics is listed in Table. 3. Results show that with obvious increasing trend ECR curve inside air, LSTM model performs worse than simpler ARIMA model due to overfitting problem. However, ECR curves inside N_2 and SF_6 gases are obvious nonlinear with much more complex deterioration behavior, LSTM model shows much better performance than other methods for its excellent time-depend nonlinear fitting ability. Thus, the proposed LSTM is suitable for ECR prediction of GIB electrical contact surrounded by SF_6, N_2 and air insulation gases.

TABLE 3. Metrics of differnet methods for single-step prediction.

Gas	Method	*RMSPE*	*MAPE*	R_{sq}
Air	ARIMA	0.013	0.010	0.998
	MLP	0.084	0.078	0.858
	CNN	0.067	0.058	0.903
	LSTM	0.031	0.028	0.981
N_2	ARIMA	0.039	0.032	0.92
	MLP	0.055	0.054	0.874
	CNN	0.021	0.016	0.977
	LSTM	0.016	0.013	0.987
SF_6	ARIMA	0.017	0.013	0.991
	MLP	0.055	0.053	0.913
	CNN	0.025	0.021	0.981
	LSTM	0.015	0.012	0.993

B. MULTI-STEP ECR PREDICTION

Multi-step ECR prediction results of GIB electrical contact inside different insulation gases are shown in Fig.11. Performance of model metrics are listed in Table.4.

Similar as results of single-step prediction. ARIMA model performs better than other models for the multi-step ECR prediction of GIB electrical contact inside air with obvious increasing trend. However, LSTM is more suitable for the multi-step ECR prediction of GIB electrical contact inside N_2 and SF_6 gases with much more complex deterioration behavior and more obvious nonlinear ECR curve Thus, proposed LSTM is suitable for multi-step ECR prediction of GIB electrical contact surrounded by SF_6, N_2 and air insulation gases.

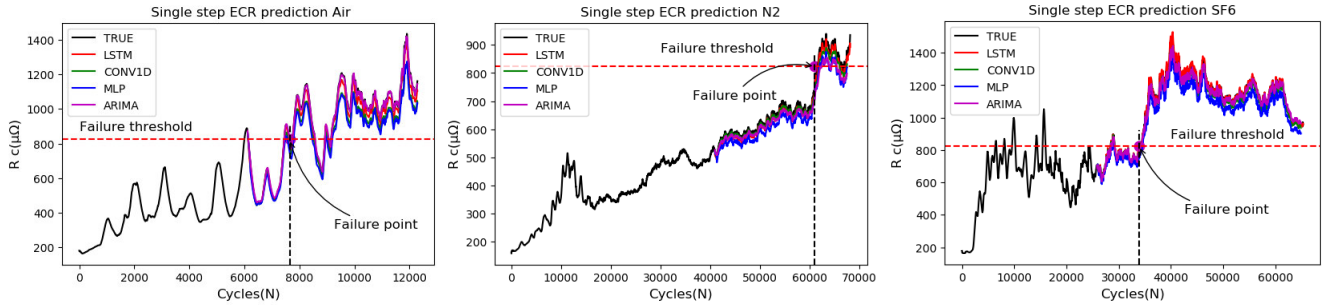

FIGURE 10. Single-step ECR prediction results of GIB electrical contact.

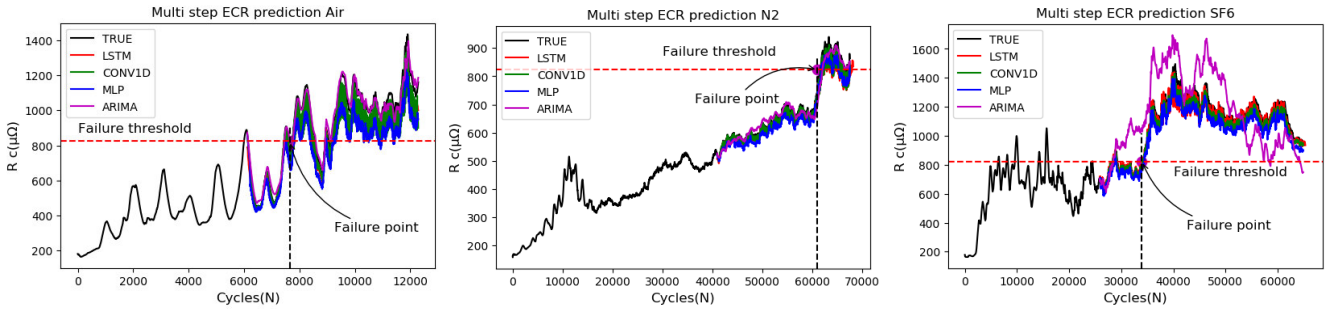

FIGURE 11. Multi-step ECR prediction results of GIB electrical contact.

TABLE 4. Metrics of differnet methods for multi-step prediction.

Gas	Method	*RMSPE*	*MAPE*	R_{sq}
Air	ARIMA	0.041	0.032	0.979
	MLP	0.136	0.128	0.645
	CNN	0.111	0.091	0.736
	LSTM	0.082	0.074	0.867
N_2	ARIMA	0.032	0.025	0.96
	MLP	0.046	0.044	0.91
	CNN	0.029	0.021	0.957
	LSTM	0.018	0.015	0.985
SF_6	ARIMA	0.207	0.175	0.062
	MLP	0.069	0.061	0.868
	CNN	0.041	0.035	0.949
	LSTM	0.042	0.035	0.949

TABLE 5. Failure prediction results of GIB electrical contact.

Gas	RUL prediction result	
Air	Single step	7661
	Multi-step	7666
	Failure point	7646
N_2	Single step	61110
	Multi-step	60876
	Failure point	60992
SF_6	Single step	33924
	Multi-step	33900
	Failure point	33942

C. ACTIVATION FUNCTION AND LOSS FUNCTION

Failure prediction results of GIB electrical contact obtained by LSTM method are listed in Table 5. Single-step and multi-step failure prediction results inside air are 15 cycles and 20 cycles after contact failure happens (failure point). RUL prediction results inside N_2 is 118 cycles after (single step) and 116 cycles before (multi-step) contact failure happens. Failure prediction results inside SF_6 is 18 cycles (single step) and 42 cycles (multi step) before failure point. Considering 3 thermal cycle loads per day [19], maximum failure prediction error for GIB electrical contact is 40 days and it is enough to make preventive maintenance.

VII. CONCLUSION

In this study, contact deterioration behavior of GIB electrical contact inside different insulation gases (SF_6, N_2 and Air) under low and high load currents (20A and 60A) are analyzed. Using defined failure threshold and measured contact resistance curve, a failure prediction method of GIB electrical contact based on LSTM is developed. This work could yield novel information for our understanding of how electrical contact deteriorate under high current load within medium other than air, and provide a sound technical support for the design, manufacturing, and condition maintenance of both air and gas insulated power equipment. Conclusions are summarized as follows.

1) Insulation gas and operation current could influence the current-carrying wear mechanisms and contact deterioration behaviors of GIB connector. Contact deterioration process inside SF_6 and N_2 gas is smaller than that in air with less oxidation effect. With increase of load current, contact deterioration inside SF_6 gas becomes more severe than N_2 gas with the formation of high resistivity fluoride and sulphide composites under local high temperature rise.

2) It is found that ECR curve of GIB electrical contact can be smoothed by EWMA to extract its long-term trend. LSTM architecture can be used to extract high dimension sequence features embedded in ECR curve. A Fc neural network can finalize ECR prediction task.

3) Compared with other time sequence prediction methods, proposed LSTM method helps obtain better single-step and multi-step failure prediction results of GIB electrical contact especially inside SF_6 gas with much more obvious nonlinear ECR deterioration process.

REFERENCES

[1] M. Runde, "Failure frequencies for high-voltage circuit breakers, disconnectors, earthing switches, instrument transformers, and gas-insulated switchgear," *IEEE Trans. Power Del.*, vol. 28, no. 1, pp. 529–530, Jan. 2013.

[2] Y. Mukaiyama, I. Takagi, K. Izumi, T. Sekiguchi, A. Kobayashi, and T. Sumikawa, "Investigation on abnormal phenomena of contacts using disconnecting switch and detachable bus in 300 kV GIB," *IEEE Trans. Power Del.*, vol. 5, no. 1, pp. 189–195, Jan. 1990.

[3] C. Pan, G. Chen, J. Tang, and K. Wu, "Numerical modeling of partial discharges in a solid dielectric-bounded cavity: A review," *IEEE Trans. Dielectr. Electr. Insul.*, vol. 26, no. 3, pp. 981–1000, Jun. 2019.

[4] X. Guan, J. Qin, N. Shu, and H. Peng, "Studies on contact degradation process and failure mechanism of GIB plug-in connector," *IEEE Trans. Compon., Packag., Manuf. Technol.*, vol. 9, no. 9, p. 1776 1784, Jul. 2019.

[5] Z. Fu, W. Chen, Z. Li, L. Xiang, C. Li, K. Bian, L. Wang, and B. Liu, "Wear mechanism and mass loss characteristic of arcing contacts in SF6 circuit breaker in making process," *IEEE Trans. Compon., Packag., Manuf. Technol.*, vol. 8, no. 9, p. 1593 1603, May 2018.

[6] H. Tian, P. Liu, S. Zhou, Q. Wang, Z. Wu, J. Zhang, and Z. Peng, "Research on the deterioration process of electrical contact structure inside the ±500 kV converter transformer RIP bushings and its prediction strategy," *IET Gener., Transmiss. Distrib.*, vol. 13, no. 12, pp. 2391–2400, Jun. 2019.

[7] Y.-Z. Lam, J. W. McBride, C. Maul, and J. K. Atkinson, "Displacement measurements at a connector contact interface employing a novel thick film sensor," *IEEE Trans. Compon. Packag. Technol.*, vol. 31, no. 3, pp. 566–573, Sep. 2008.

[8] C. H. Leung and A. Lee, "Thermal cycling induced wiping wear of connector contacts at 150/spl deg/C," *IEEE Trans. Compon. Packag. Technol.*, vol. 22, no. 1, pp. 72–78, Mar. 1999.

[9] Y. Zhang, Y. Zhang, and C. Song, "Arc discharges of a pure carbon strip affected by dynamic contact force during current-carrying sliding," *Materials*, vol. 11, no. 5, p. 796, May 2018.

[10] V. V. Fadina, M. I. Aleutdinovaa, and A. V. Kolubaeva, "Effect of high-density electric current on wear and average temperature of steel/steel triboelectric contact," *J. Friction Wear*, vol. 39, no. 4, pp. 370–375, Aug. 2018.

[11] H. Mishina, "Atmospheric characteristics in friction and wear of metals," *Wear*, vol. 152, no. 1, pp. 99–110, Jan. 1992.

[12] Å. Kassman Rudolphi and S. Jacobson, "Stationary loading, fretting and sliding of silver coated copper contacts—Influence of corrosion films and corrosive atmosphere," *Tribology Int.*, vol. 30, no. 3, pp. 165–175, Mar. 1997.

[13] B. H. Chudnovsky, "Corrosion of electrical conductors in pulp and paper industrial applications," *IEEE Trans. Ind. Appl.*, vol. 44, no. 3, pp. 932–939, May 2008.

[14] X.-L. Liu, Z.-B. Cai, Y. Cui, S.-B. Liu, X.-J. Xu, and M.-H. Zhu, "Effect of different atmospheres on the electrical contact performance of electronic components under fretting wear," *J. Phys. D, Appl. Phys.*, vol. 51, no. 15, Mar. 2018, Art. no. 155302.

[15] B. Sun, Y. Li, Z. Wang, Y. Ren, Q. Feng, D. Yang, M. Lu, and X. Chen, "Remaining useful life prediction of aviation circular electrical connectors using vibration-induced physical model and particle filtering method," *Microelectron. Rel.*, vol. 92, pp. 114–122, Jan. 2019.

[16] Q. Li, K. Lv, J. Qiu, and G. Liu, "Research on residual life prediction for electrical connectors based on intermittent failure and hidden semi-Markov model," *Appl. Sci.*, vol. 8, no. 8, p. 1373, Aug. 2018.

[17] S. Fouvry, P. Jedrzejczyk, O. Perrinet, O. Alquier, and P. Chalandon, "Introduction of a 'Modified archard wear law' to predict the electrical contact endurance of thin plated silver coatings subjected to fretting wear," in *Proc. IEEE 58th Holm Conf. Electr. Contacts (Holm)*, Sep. 2012, pp. 1–13.

[18] H. Cui, Z. Wu, G. Wu, X. Xu, Y. You, and Y. Fang, "Convolutional neural networks for electrical endurance prediction of alternating current contactors," *IEEE Trans. Compon., Packag., Manuf. Technol.*, vol. 9, no. 9, pp. 1785–1793, Sep. 2019.

[19] A. E. Emanuel, H. C. Doepken, and P. C. Bolin, "Design and test of a sliding plug-in conductor connector for compressed gas-insulated cables," *IEEE Trans. Power App. Syst.*, vol. PAS-95, no. 2, pp. 570–579, Mar. 1976.

[20] H. Shinkai, H. Goshima, and Y. Masafumi, "A study on condition assessment method of gas-insulated switchgear—Part II. Influence of moisture in the SF_6, detection of a partial discharge on a spacer, repetition discharge and overheating by incomplete contact," *Electr. Eng. Jpn.*, vol. 176, no. 2, pp. 174–182, Apr. 2011.

[21] J. Tang, J. Pan1, Q. Yao, Y. Miao, X. Huang, and F. Zeng, "Feature extraction of SF_6 thermal decomposition characteristics to diagnose overheating fault," *IET Sci., Meas. Technol.*, vol. 9, no. 6, pp. 174–182, Sep. 2015.

[22] J. Wang, W. Ding, J. Yan, Y. Wang, Y. Wang, Z. Li, and G. Li, "Decomposition characteristics of SF6 under overheating conditions," *IEEE Trans. Dielectr. Electr. Insul.*, vol. 24, no. 6, pp. 3405–3415, Dec. 2017.

[23] *High-Voltage Switchgear and Control Gear—Part 1: Common Specifications*, Standard IEC62271-1 Edition 1.1 2011-08, 2011.

[24] R. Holm, *Electric Contacts, Theory and Applications*. New York, NY, USA: Springer, 1979.

[25] L. Bin, *SF6 High Voltage Electrical Design*. Beijing, China: China Machine Press, 2007.

[26] S. Hochreiter and J. Schmidhuber, "Long short-term memory," *Neural Comput.*, vol. 9, no. 8, pp. 1735–1780, 1997.

XIANGYU GUAN received the B.S. degree in environmental science from Xinjiang Normal University, Urumqi, China, in 2010, and the M.S. and Ph.D. degrees in electrical engineering from Wuhan University, Wuhan, China, in 2015.

From 2016 to 2018, he worked as a Postdoctoral Researcher with the School of Electrical Engineering, Wuhan University. He is currently a Lecturer with the College of Electrical Engineering and Automation, Fuzhou University, Fuzhou, China. His research interests include the numerical methods of coupling field calculation and the condition monitoring of electrical equipment. He is a member of the ACES and ICS.

YUEQUAN WEN, photograph and biography not available at the time of publication.

ZHE DONG, photograph and biography not available at the time of publication.

NAIQIU SHU received the M.S. and Ph.D. degrees from the College of Electrical Engineering, Wuhan University, Wuhan, China. He is a Professor with the College of Electrical Engineering, Wuhan University. His research interest includes the condition monitoring of electrical equipment.

HUI PENG received the B.S., M.S., and Ph.D. degrees in electrical engineering from Wuhan University, Wuhan, China. He is an Associate Professor with the School of Electrical Engineering, Wuhan University. His current research interest includes the condition monitoring of electrical equipment.

WEI GAO, photograph and biography not available at the time of publication.

DAVID WENZHONG GAO (Senior Member, IEEE) received the M.S. and Ph.D. degrees in electrical and computer engineering, specializing in electric power engineering, from the Georgia Institute of Technology, Atlanta, USA, in 1999 and 2002, respectively.

He is currently with the Department of Electrical and Computer Engineering, University of Denver, CO, USA. His current teaching and research interests include renewable energy and distributed generation, microgrid, smart grid, power system protection, power electronics applications in power systems, power system modeling and simulation, and hybrid-electric propulsion systems. He was the General Chair of the IEEE Symposium on Power Electronics and Machines in Wind Applications (PEMWA) in 2012 and the 48th North American Power Symposium (NAPS) in 2016. He is an Editor of the IEEE TRANSACTIONS ON SUSTAINABLE ENERGY.